RACGAP1 defines a malignant proliferative niche and represents a therapeutic vulnerability in lung adenocarcinoma

Ming Yi[1#], Jiaying Shi[2,3#], Shengyu Xie[2], Dachang Tao[2], Zhiguang Su[1], Yuan Yang[2], Yunqiang Liu[2]

[1]Center for High Altitude Medicine, Frontiers Science Center for Disease-related Molecular Network, State Key Laboratory of Biotherapy, West China Hospital, Sichuan University, Chengdu, China; [2]Department of Medical Genetics, State Key Laboratory of Biotherapy, West China Hospital, Sichuan University, Chengdu, China; [3]Department of Rehabilitation Medicine, Xuanwu Hospital, Capital Medical University, Beijing, China

Contributions: (I) Conception and design: M Yi, J Shi, Y Liu; (II) Administrative support: D Tao, Y Liu; (III) Provision of study materials or patients: None; (IV) Collection and assembly of data: M Yi, J Shi, S Xie; (V) Data analysis and interpretation: M Yi, J Shi, S Xie; (VI) Manuscript writing: All authors; (VII) Final approval of manuscript: All authors.

[#]These authors contributed equally to this work.

Correspondence to: Yunqiang Liu, PhD. Department of Medical Genetics, State Key Laboratory of Biotherapy, West China Hospital, Sichuan University, No. 37 Guoxue Alley, Wuhou District, Chengdu 610041, China. Email: yq_liu@scu.edu.cn.

Background: The clinical management of lung adenocarcinoma (LUAD) is compromised by post-surgical recurrence and therapeutic resistance, underscoring the urgent need to uncover actionable therapeutic vulnerabilities. By integrating human genetics with multi-omics profiling and experimental validation, this study aims to systematically uncover critical molecular mediators of LUAD and delineate their therapeutic potential.

Methods: We implemented a multi-modal framework to identify and characterize causal LUAD therapeutic targets. We used two-sample Mendelian randomization (2SMR) to identify plasma proteins that are causally linked to LUAD risk. The lead candidate was then investigated using multi-omics to delineate its clinical relevance, cellular drivers, and tumor microenvironment. Oncogenic mechanisms were subsequently interrogated through functional experiments in LUAD models.

Results: Our unbiased genetic screen identified Rac GTPase-activating protein 1 (RACGAP1) as a high-confidence causal risk factor for LUAD. Clinically, elevated RACGAP1 expression served as a robust, independent prognostic biomarker associated with poor survival across multiple cohorts. Single-cell profiling revealed that *RACGAP1* defines a specific expanding epithelial subpopulation characterized by chromosomal instability (CIN) and apoptosis resistance. Spatially, these cells organize into "malignant proliferative niches" that drive tumor expansion. Mechanistically, RACGAP1 transcends its canonical role in cytokinesis to function as a pivotal oncogenic hub. It disables p53-mediated tumor suppression by upregulating MDM2, while concurrently activating the pro-survival PI3K/AKT and MEK/ERK signaling cascades. Crucially, pharmacological inhibition of these pathways abrogated the RACGAP1-driven malignant phenotypes, confirming the functional dependence of the tumor on this rewired signaling architecture.

Conclusions: This study presents genetic evidence supportive of a causal contribution of RACGAP1 to LUAD, highlighting it as a promising prognostic biomarker and candidate therapeutic target. By delineating a RACGAP1-driven axis that coordinates survival signaling and suppresses tumor surveillance, our findings highlight RACGAP1 as a promising therapeutic target for novel adjuvant strategies.

Keywords: Biomarker; causal inference; integrated multi-omics strategy; spatial omics; lung adenocarcinoma (LUAD)

Submitted Oct 10, 2025. Accepted for publication Dec 15, 2025. Published online Jan 26, 2026.
doi: 10.21037/tlcr-2025-aw-1158
View this article at: https://dx.doi.org/10.21037/tlcr-2025-aw-1158

Introduction

Lung adenocarcinoma (LUAD) is a leading cause of cancer-related mortality worldwide (1,2). Although targeted therapies have improved patient outcomes, the inevitable emergence of drug resistance and tumor recurrence underscores the urgent need for novel therapeutic strategies (3-5). A central challenge in this pursuit is to distinguish causal drivers of pathogenesis from disease-associated molecules (6). Therefore, identifying and validating targets with a strong genetic and biological basis for causality is of paramount priority.

Plasma proteins, which serve as essential mediators of cellular processes including signal transduction, molecular transport, and proliferation, represent a rich source of potential biomarkers and therapeutic targets (7). Recent advances in large-scale proteomic-genetic association studies have identified numerous protein quantitative trait loci (pQTLs) (8), enabling the use of Mendelian randomization (MR) to infer causal relationships between protein levels and disease risk (9-12). By leveraging genetic variants as instrumental variables (IVs), MR can effectively mitigate confounding and reverse causality (13), thereby offering a powerful tool for causal inference. However, establishing a genetic link with disease risk is the first step. This approach does not resolve the protein's mechanistic role, cellular context within the tumor microenvironment, or its value as a prognostic biomarker. Furthermore, traditional bulk-tissue analyses are limited by cellular heterogeneity, which can obscure the specific cell populations responsible for oncogenic signals.

To bridge these critical gaps, we designed and implemented an integrative multi-omics framework. Our strategy begins with a genetic-driven approach, using two-sample MR (2SMR) and colocalization to identify plasma proteins causally associated with LUAD risk. We then integrated the clinical data to assess the prognostic relevance of these candidates. Finally, we employed single-cell and spatial transcriptomics to dissect the cell-type specific functions of candidate proteins and their spatial organization within the tumor niche, followed by mechanistic validation. This systematic approach allows for the triangulation of evidence from human genetics, clinical outcomes, and tumor biology to identify and deeply characterize highly reliable potential therapeutic targets in LUAD. We present this article in accordance with the MDAR and STROBE-MR reporting checklists (available at https://tlcr.amegroups.com/article/view/10.21037/tlcr-2025-aw-1158/rc).

Highlight box

Key findings

- This study provides genetic evidence supportive of a causal contribution of Rac GTPase-activating protein 1 (RACGAP1) to lung adenocarcinoma (LUAD) pathogenesis, moving beyond prior correlational reports. We identified a malignant *RACGAP1*$^{+}$ epithelial niche that drives tumor aggressiveness through enhanced proliferation and apoptosis resistance. Mechanistically, RACGAP1 orchestrates a dual oncogenic program—disabling p53-mediated tumor suppression while activating PI3K/MEK pro-survival signaling. This work defines the RACGAP1 axis as a critical, actionable vulnerability in high-risk LUAD.

What is known and what is new?

- While elevated RACGAP1 expression is known to correlate with poor prognosis in LUAD, its causal role is unproven.
- This study provides the first genetic evidence identifying RACGAP1 as an intrinsic causal factor in LUAD pathogenesis. We map this effect to a specific malignant niche and uncover a dual mechanism (p53 inactivation/survival pathway activation) that sustains tumor aggression.

What is the implication, and what should change now?

- These findings highlight RACGAP1 as a robust prognostic biomarker and a promising candidate for therapeutic exploration. The dependency of the malignant niche on the RACGAP1 axis presents a critical, exploitable vulnerability.
- Research should now pivot to validating RACGAP1 inhibition in clinical contexts. Specifically, targeting this axis offers a rational strategy for the adjuvant setting to mitigate recurrence and improve survival in high-risk, post-surgical LUAD patients.

Methods

Detailed methodologies are provided in Appendix 1, including data sourcing, single-cell data quality control (QC) and preprocessing (clinical characteristics in Table S1), copy number variation (CNV) inference, and spatial transcriptomics. For *in vitro* experiments, methodologies for cell culture, 5-ethynyl-2'-deoxyuridine (EdU), colony formation, reverse transcription-quantitative polymerase chain reaction (RT-qPCR) (primer sequences in Table S2), and Western blot (primary antibody details in Table S3) are also provided. This study was conducted in accordance with the Declaration of Helsinki and its subsequent amendments. The bioinformatic analyses in this study were conducted using publicly available datasets. All datasets utilized were generated by studies that had previously obtained ethical approval from their respective institutional review boards

(IRBs). Informed consent was obtained from all participants as part of these original data collection efforts. Therefore, the current study was deemed exempt from IRB approval by the Ethics Committee of West China Hospital in Sichuan University.

Study design

We implemented a multi-stage framework to identify and validate the causal drivers of LUAD by integrating genetic, clinical, and experimental evidence (*Figure 1A*). First, we employed 2SMR and Bayesian colocalization to identify plasma proteins that were causally associated with LUAD risk. The prognostic significance of these candidate proteins was then evaluated in patient cohorts via Cox proportional hazards models, Kaplan-Meier (KM) survival analysis, and differential gene expression. Subsequently, the lead candidate was characterized using single-cell and spatial transcriptomics to delineate its expression pattern and microenvironmental niche. Finally, its oncogenic functions and downstream signaling pathways were validated through gain- and loss-of-function experiments using LUAD models.

Instrument selection

Genetic instruments for plasma proteins were derived from the deCODE project (14). We selected cis-acting single-nucleotide polymorphisms (SNPs) with a genome-wide significance ($P<5\times10^{-8}$) as initial IVs. To ensure robustness, we excluded IVs associated with potential confounders and retained only strong instruments (*F*-statistic >10) to mitigate the weak instrument bias. The final set of SNPs used in our 2SMR analysis is presented in Table S4.

Bayesian colocalization analyses

To assess the probability that two traits share a causal genetic variant at a given locus, we performed Bayesian colocalization analysis using the R package 'coloc' (15). This method computes the posterior probability (PP) for five competing hypotheses: no association (H0), association with only trait 1 (H1) or trait 2 (H2), association with distinct causal variants (H3), and a shared causal variant (H4). We defined strong evidence of colocalization as a PP for H4 (PPH4) of ≥0.8.

2SMR analysis

Our 2SMR analysis relies on three core assumptions: (I) IVs are robustly associated with plasma protein levels; (II) IVs are independent of confounders; and (III) IVs affect LUAD risk only through protein levels, precluding horizontal pleiotropy. For each protein, we selected the lead SNP with the maximum Z-score as the single IV. When a primary IV was absent from the LUAD outcome data, we identified a proxy SNP from the 1000 Genomes European panel (linkage disequilibrium $R^2\geq0.8$). IVs lacking a suitable proxy were excluded to ensure the validity of causal estimates (16). Causal effects were estimated using the Wald ratio method, and results were expressed as odds ratios (ORs) with 95% confidence intervals (CIs). To correct for multiple comparisons, we applied the Benjamini-Hochberg procedure to control the false discovery rate (FDR) at 5%. The formula for calculating R^2 has been described elsewhere (17):

$$R^2=\frac{\beta^2}{\beta^2+N\times se^2} \quad [1]$$

where β represents the SNP effect size, N represents the sample size of the genome-wide association study (GWAS) exposure data, and se indicates the standard error of the effect estimate. To assess IVs strength, we further calculated the *F*-statistic using the following formula (17):

$$F=\frac{R^2}{1-R^2}\times\left(N-K-1/K\right) \quad [2]$$

where R^2 represents the variance in the exposure explained by the IVs, N represents the sample size of the exposure GWAS data, and K represents the number of IVs.

All MR analyses adhered to the MR-STROBE guidelines (18).

Cox regression, KM, and differential gene expression analysis

The association between individual gene expression and patient survival was initially evaluated using a univariable Cox regression analysis. Genes identified as significant were subsequently included in a multivariable Cox regression model, which was adjusted for established clinicopathological factors (age, gender, and pathologic stage) to assess their independent prognostic value. KM curves were generated to visualize survival differences. In

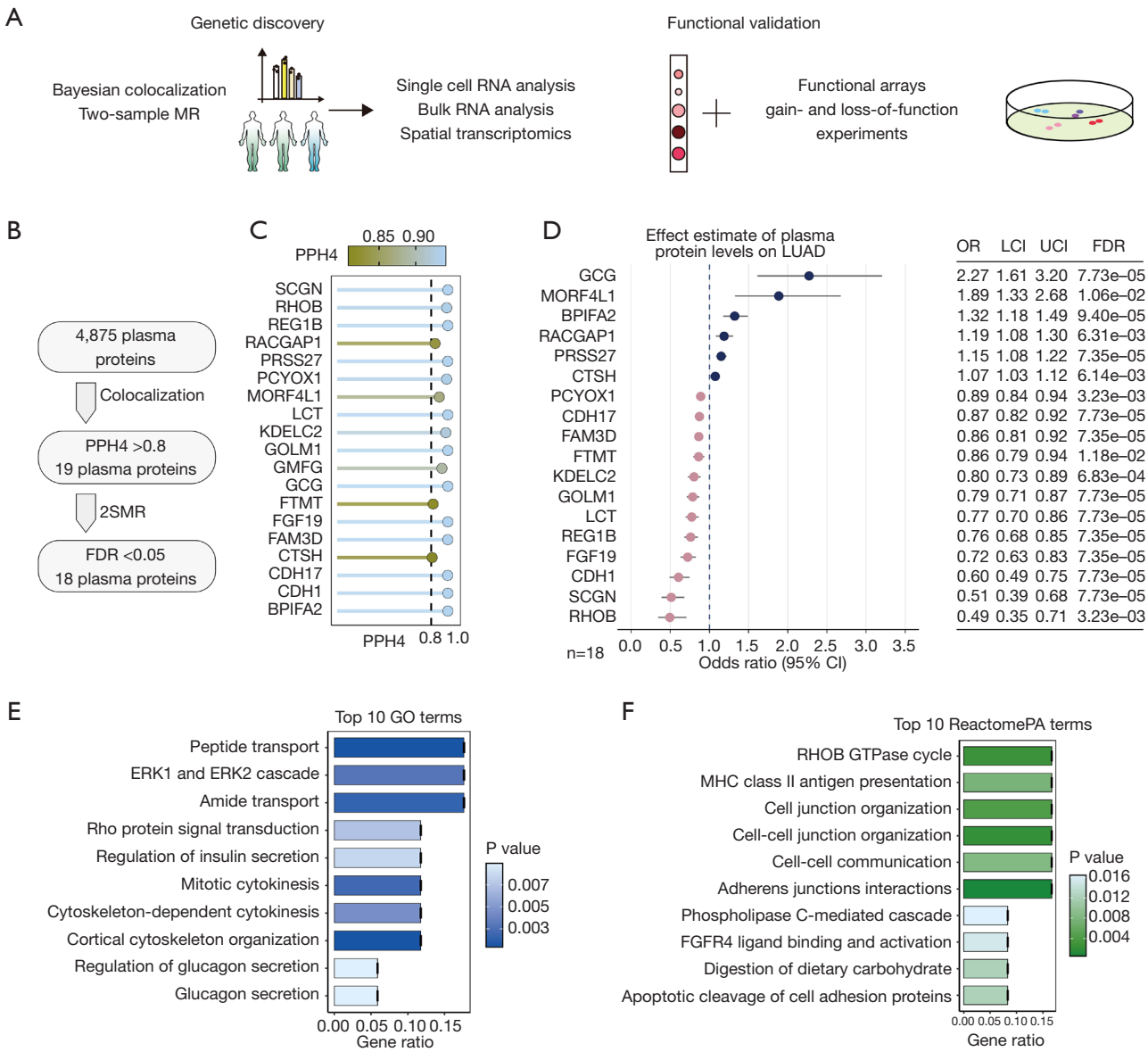

Figure 1 Prioritizing putative causal proteins for LUAD through systematic genetic analysis. (A,B) Schematic workflow for identifying plasma proteins causally associated with LUAD. A total of 4,875 plasma proteins were first subjected to colocalization analysis. Proteins with strong evidence of colocalization (PPH4 >0.8) were selected (n=19) and further analyzed using 2SMR. Proteins showing significant associations after multiple testing correction (FDR <0.05) were retained (n=18). (C) Colocalization analysis of candidate plasma proteins with LUAD genetic loci. The horizontal axis shows the PPH of colocalization (PPH4) for each protein. The color bar indicates PPH4 values. (D) Forest plots showing the results from 2SMR analysis. (E,F) GO term and Reactome pathway enrichment analyses. 2SMR, two-sample Mendelian randomization; CI, confidence interval; FDR, false discovery rate; GO, Gene Ontology; LCI, lower 95% CI of OR; LUAD, lung adenocarcinoma; OR, odds ratio; PP, posterior probability; PPH4, posterior probability for H4; UCI, upper 95% CI of OR.

parallel, differential gene expression analysis was conducted to identify genes with altered expression between groups. All survival analyses were performed using the R package glmnet (version 4.1-7).

Cell type annotation and differential gene identification

After QC (Figure S1A) and stringent batch correction (Figure S1B), we performed differential gene expression analysis using the Wilcoxon rank-sum test in the SCANPY package. Subsequently, major cell types were annotated based on the expression of canonical marker genes (19-21) as follows: *CD3D* and *TRAC* for T cells, *LYZ* and *CD14* for myeloid cells, *CD79A* and *MS4A1* for B cells, *GNLY* and *NKG7* for natural killer (NK) cells, *MZB1* and *JCHAIN* for plasma cells, *EPCAM* and *KRT18* for epithelial cells, *COL1A1* and *DCN* for fibroblasts, *CDH5* and *VWF* for endothelial cells, *CAP3* and *TPSAB1* for mast cells, and *PLP1* and *MOG* for oligodendrocytes (Figure S1C).

Gene set enrichment analysis (GSEA) and gene set variation analysis (GSVA)

GSEA was performed to identify pre-defined gene sets showing significant concordant differences between phenotypes. This analysis utilized the clusterProfiler R package (22) with the complete ranked list of expressed genes as input. To quantify the pathway activity for individual samples, GSVA was conducted using the GSVA R package (23). This method converts the gene-by-sample expression matrix into a pathway-by-sample enrichment score matrix, which enables the comparison of relative pathway activity across different groups.

Cell viability assessment

Cell viability was quantitatively evaluated using the Cell Counting Kit-8 (CCK-8) assay (Bioground, Chongqing, China) according to the manufacturer's protocol. A549 cells were seeded at a density of 3×10^3 cells per well in 96-well plates and allowed to adhere overnight. Following treatment at the designated time points (0, 24, 48, and 72 h), 10 µL of CCK-8 reagent was added to each well, and cells were incubated for 2 h at 37 ℃ in a humidified atmosphere containing 5% CO_2. Optical density was measured at 450 nm using a microplate reader (Thermo Scientific, Waltham, MA, USA). The assay was performed in five independent biological replicates.

Cell cycle distribution analysis

A549 cells were harvested, washed with phosphate-buffered saline (PBS), and fixed in 70% ice-cold ethanol overnight at 4 ℃. Fixed cells were resuspended in propidium iodide (PI) staining solution (50 µg/mL PI, 200 µg/mL RNase A, 0.1% Triton X-100 in PBS) and incubated for 30 min at room temperature in darkness. After filtration through 70 µm strainers, data were acquired using a BD FACSCalibur flow cytometer. Cell cycle distribution was analyzed using ModFit LT software to determine G1, S, and G2/M phase percentages. The experiment was conducted with three independent biological replicates.

Apoptosis detection

Apoptosis was assessed using the Annexin V-fluorescein isothiocyanate (FITC)/PI kit (US Everbright, Suzhou, China). Cells were harvested, washed with ice-cold PBS, and resuspended in 1× binding buffer (1×10^6 cells/mL). Cell suspensions (100 µL) were stained with Annexin V-allophycocyanin (APC) (1 µL) and PI (2 µL) for 15 min at room temperature in darkness. Flow cytometric analysis was performed within 1 h using a BD FACSCalibur, and apoptotic populations were quantified using FlowJo software with ≥10,000 events analyzed per sample. This experiment was repeated in three independent biological replicates.

Statistical analysis and visualization

In the 2SMR analysis using a single IV, the causal effect was estimated via the Wald ratio. Group comparisons were conducted using the Wilcoxon rank-sum test for two groups and the Kruskal-Wallis test for more than two groups. The statistical analysis and plotting modules in the R environment included the following: base package (version 4.2.3), TwoSampleMR package (version 0.5.7), ggstats package (version 0.3.0), data.table package (version 1.14.8), dplyr package (version 1.1.3), future package (version 1.33.1), gwasglue package (version 0.0.0.9000), gwasvcf package (version 0.1.1), Matrix package (version 1.6-1.1), ggplot2 package (version 3.4.2), circlize package (version 0.4.15), ComplexHeatmap package (version 4.2.3), ggsci package (version 3.0.0), ggpubr package (version 0.6.0), ggrepel package (version 0.9.4), and patchwork package (version 1.1.2). The statistical analysis and plotting modules in the Python environment include: the NumPy

module (version 1.24.4), pandas module (version 1.5.3), SCANPY module (version 1.9.3), anndata module (version 0.9.1), scipy module (version 1.10.1), scikit-learn module (version 1.3.0), and Statsmodels module (version 0.14.0). All *in vitro* experiments were performed with at least three biological replicates. Analysis of images was performed by an investigator blinded to the experimental conditions.

Results

Prioritizing putative causal proteins for LUAD through systematic genetic analysis

To systematically prioritize circulating proteins causally implicated in LUAD, we implemented a multi-stage genetic validation framework. We began with a proteome-wide Bayesian colocalization screen of 4,875 proteins. This step identified 19 high-confidence candidates that likely shared a common causal variant with LUAD (PPH4 >0.8) (*Figure 1B,1C*). To formally test for causality and quantify the effect size, these candidates were then subjected to the 2SMR. By leveraging genetic variants as unconfounded IVs, this analysis provided genetic evidence for the causal effect of 18 among the 19 proteins on LUAD risk (FDR <0.05; *Figure 1D*). Detailed statistics for all 18 identified proteins are provided in *Figure 1D*. Notably, Rac GTPase-activating protein 1 (RACGAP1) exhibited a significant causal association with increased LUAD risk (OR =1.19; 95% CI: 1.08–1.30; FDR =0.0063). We further validated the presumed causal directionality using MR-Steiger filtering. This confirmed that genetic instruments influenced LUAD risk primarily through their effect on protein abundance (Table S5).

To translate these genetic findings into biological insight, pathway enrichment analysis of 18 proteins with evidence of causality was performed. The analysis revealed that these proteins converge on core biological networks integral to LUAD pathogenesis (*Figure 1E,1F*). Enriched pathways included cellular transport (peptide and amide), signal transduction (ERK1/ERK2 and RHOB GTPase), cytoskeletal dynamics (mitosis and cytokinesis), and immune surveillance [major histocompatibility complex (MHC) class II antigen presentation]. Our study not only highlighted potential therapeutic targets for LUAD with supportive genetic evidence but also linked them to biologically relevant contexts.

Tissue-level multi-cohort analysis identifies RACGAP1 as a generalizable and independent prognostic biomarker in LUAD

To translate our genetic findings on disease risk into prognostic relevance, we investigated the clinical impact of 18 candidates within LUAD. First, we interrogated transcriptomic profiles in The Cancer Genome Atlas (TCGA)-LUAD cohort. Univariable Cox regression analysis and KM analysis showed that high expression of *RACGAP1*, *GOLM1*, and *CDH17*, coupled with low expression of *CTSH*, correlated with poor overall survival (*Figure 2A,2B*; Figure S2A). Subsequent multivariable Cox regression validated *RACGAP1*, *CTSH*, and *CDH17* as independent prognostic indicators (*Figure 2A*).

Next, we compared transcript and protein levels between tumor and adjacent non-cancerous tissues. This analysis revealed concordant upregulation of RACGAP1 and GOLM1, and downregulation of CTSH, at both molecular levels (*Figure 2C,2D*; Figure S2B,S2C). Notably, the prognostic significance of CDH17 was confined to the transcript level, as its protein abundance remained unchanged. To identify the robustness and generalization of these predictors, we performed multi-cohort validation. This analysis confirmed that *RACGAP1* consistently and independently predicted poor LUAD patient outcomes (*Figure 2E*; Figure S2D). To assess the clinical utility of *RACGAP1*, we calculated the incremental prognostic value using Harrell's concordance index (C-index). The addition of *RACGAP1* to a baseline clinical model significantly improved the C-index in the TCGA cohort (0.666 *vs.* 0.681, P=0.004). This incremental value was validated in four independent cohorts: GSE13213 (ΔC=0.035, P=0.005), GSE31210 (ΔC=0.019, P=0.03), GSE50081 (ΔC=0.028, P=0.042), and GSE68465 (ΔC=0.022, P<0.001). These results confirmed that *RACGAP1* adds independent prognostic power beyond standard clinical variables (Figure S3). Collectively, these results establish RACGAP1 as a highly robust and clinically relevant prognostic biomarker.

RACGAP1 expression defines a malignant epithelial subpopulation that expands with LUAD progression

Although RACGAP1 has been established as a robust and generalizable prognostic signature, this finding is confounded by cellular heterogeneity that obscures the

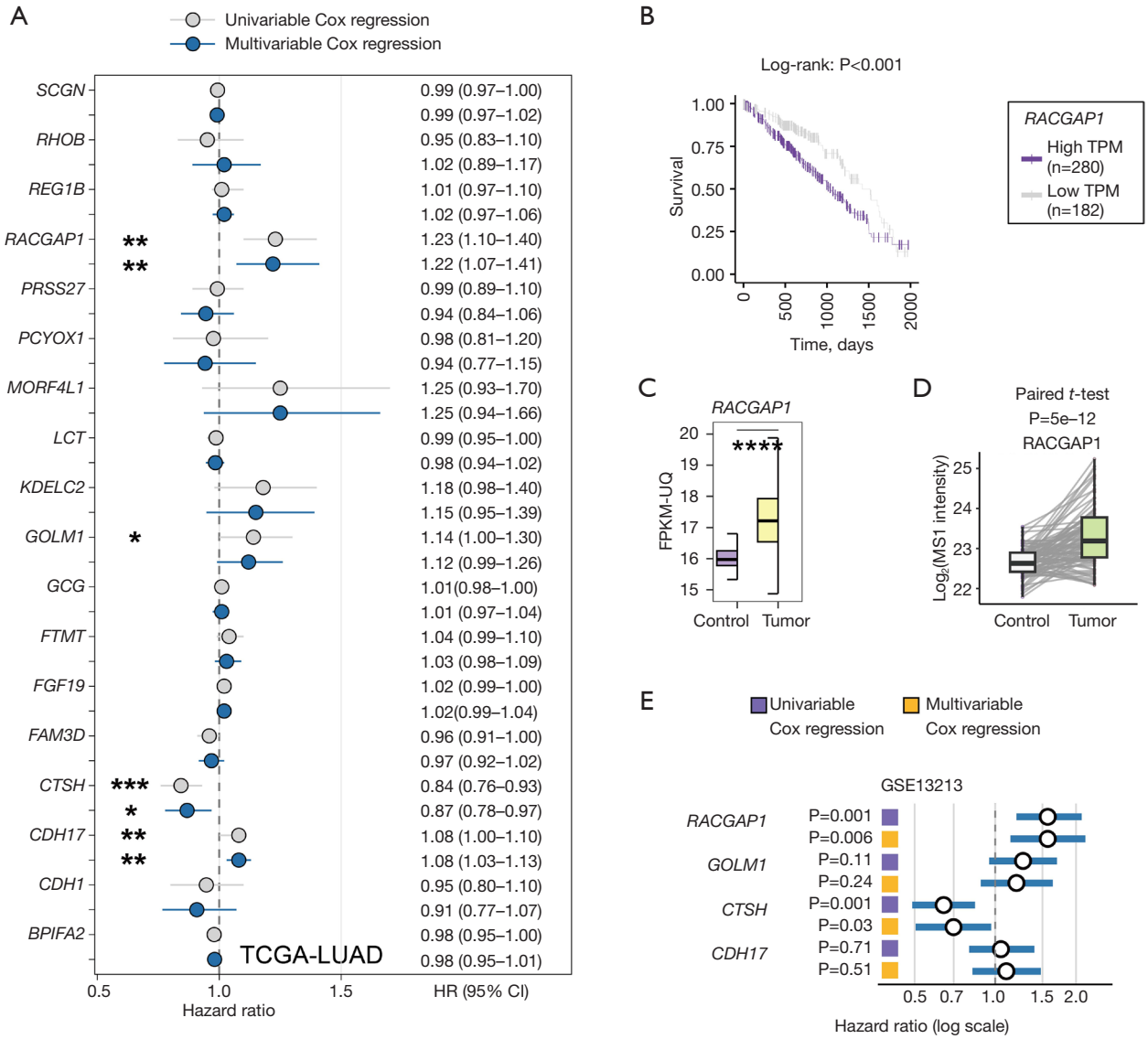

Figure 2 Tissue-level validation identifies RACGAP1 as a generalizable and independent prognostic biomarker in LUAD. (A) Forest plots showing the results from univariable and multivariable Cox proportional hazards regression analysis for OS associated with *RACGAP1* in the primary cohort. (B) KM survival curves for OS, with patients stratified by high *vs.* low mRNA expression levels of *RACGAP1*. (C,D) Differential expression profiles of RACGAP1. Comparison of (C) mRNA and (D) protein levels in tumor *vs.* adjacent non-tumor tissues. (E) Validation of the prognostic signature in the independent external LUAD cohorts, displaying results from univariable and multivariable Cox regression analyses. Statistical significance is indicated as follows: *, P<0.05; **, P<0.01; ***, P<0.001; ****, P<0.0001. CI, confidence interval; FPKM, fragments per kilobase of transcript per million fragments mapped; HR, hazard ratio; KM, Kaplan-Meier; LUAD, lung adenocarcinoma; mRNA, messenger RNA; MS, mass spectrometry; OS, overall survival; RACGAP1, Rac GTPase-activating protein 1; TCGA, The Cancer Genome Atlas; TPM, transcripts per million; UQ, upper quartile.

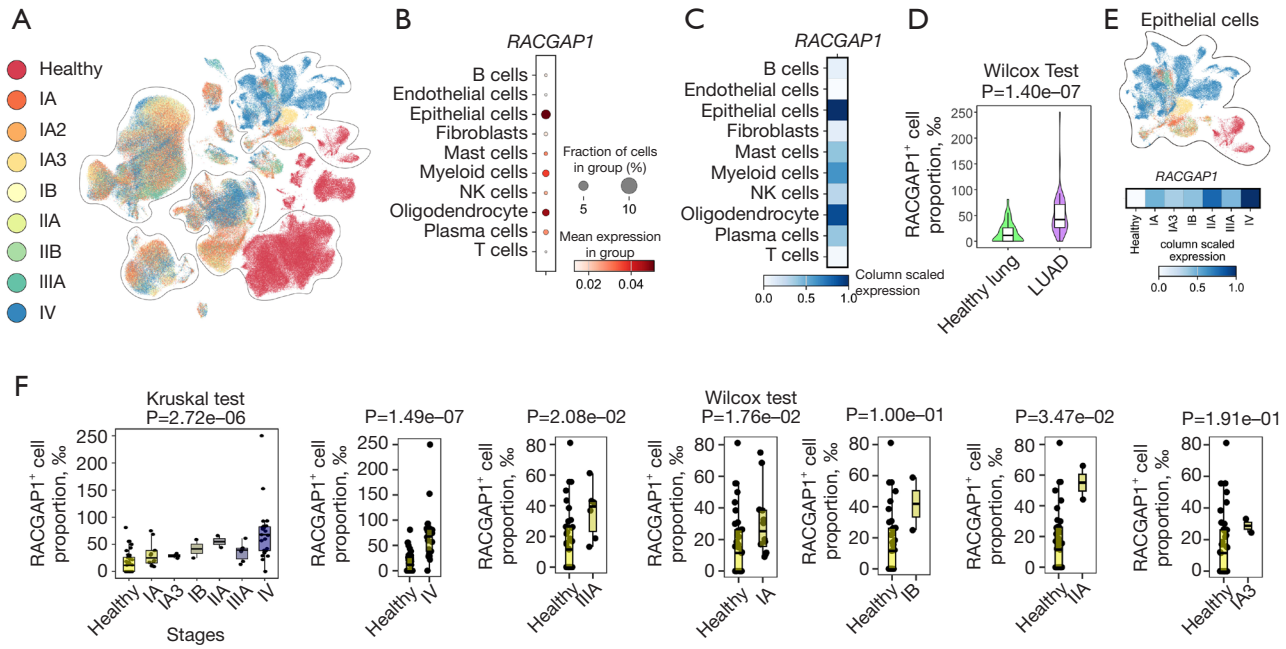

Figure 3 Single-cell analysis of tissue samples revealed distinct cell populations and their marker profiles. (A) UMAP visualization demonstrating the distribution of identified cell populations in two-dimensional space. Cells are colored by tumor stage. (B,C) Dot plot and heatmap showing the expression of *RACGAP1* in different cells. (D) Violin plots showing a significant enrichment of *RACGAP1*$^+$ epithelial cells in LUAD patients *vs.* healthy controls. (E) Correlation of *RACGAP1* with disease progression, showing a stepwise increase in both its average expression level and the proportion of *RACGAP1*$^+$ epithelial cells with advancing tumor stage. (F) Boxplot showing the proportion of *RACGAP1*$^+$ epithelial cells between multiple tumor stages and healthy controls. Statistical tests revealed a significant increase in this proportion in tumor stages compared to the healthy group. LUAD, lung adenocarcinoma; NK, natural killer; RACGAP1, Rac GTPase-activating protein 1; UMAP, Uniform Manifold Approximation and Projection.

specific cell types driving this association. To resolve this, we performed an integrative single-cell RNA sequencing (scRNA-seq) analysis of 95 clinical samples. After stringent QC and batch correction, we constructed a cellular atlas comprising 10 major lineages (Figure S4) (21,24).

Expression mapping localized *RACGAP1* predominantly to the epithelial lineage (*Figure 3A-3C*). Within this lineage, we observed a significantly higher proportion of *RACGAP1*$^+$ cells in LUAD samples compared to healthy controls (*Figure 3D*). Furthermore, this enrichment correlated with disease progression. Both the mean *RACGAP1* expression and the proportion of *RACGAP1*$^+$ cells increased progressively with advancing LUAD stages (*Figure 3E,3F*).

Collectively, these findings demonstrated that the expansion of a *RACGAP1*$^+$ epithelial subpopulation is a hallmark of LUAD progression. This suggests that these cells are critical drivers of malignancy.

RACGAP1 correlates with proliferation and genomic instability in malignant epithelial cells

To mechanistically link the expansion of *RACGAP1*$^+$ epithelial cells to LUAD progression, we first characterized the genomic landscape of single epithelial cells by inferring copy number variations. This analysis revealed widespread patterns of chromosomal aberrations indicative of malignant transformation (*Figure 4A*). These malignant cells exhibited hallmark oncogenic phenotypes, including evasion of apoptosis and augmented proliferation (*Figure 4B*). Crucially, both the mean expression of *RACGAP1* and the percentage of *RACGAP1*$^+$ cells were significantly elevated within this malignant population (*Figure 4C*).

RACGAP1 functions as a pivotal subunit of the evolutionary conserved centralspindlin complex, a

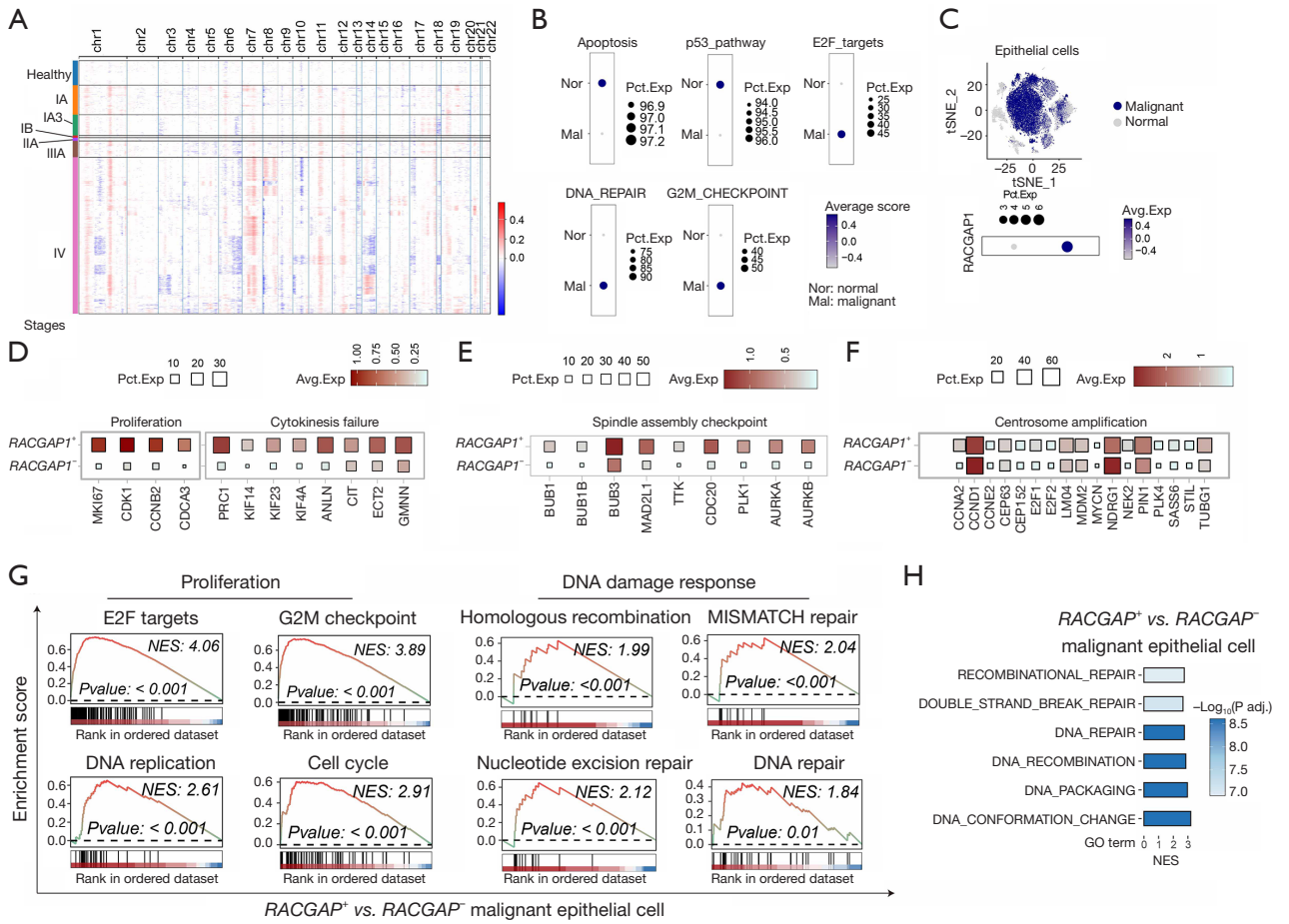

Figure 4 *RACGAP1* drives malignancy by simultaneously promoting cell cycle progression and inducing CIN. (A) CNV profiles were inferred from the scRNA-seq data of individual epithelial cells derived from healthy lung tissue and LUAD tumors. The resulting heatmap visualizes chromosomal gains (red) and losses (blue) across the genome. Individual cells (Y-axis) are stratified by patient subgroup, while genomic loci (X-axis) are arranged by chromosomal position. (B) Mean enrichment score (color) and percentage of expressing cells (size) for cancer hallmark gene sets. (C) t-SNE plot distinguishing malignant and normal epithelial cell populations. Dot plot of *RACGAP1* expression. Dot color denotes the mean expression level, and dot size denotes the percentage of expressing cells for each population. (D-F) Dot plot of transcriptional signatures related to cell proliferation, cytokinesis, spindle assembly, and centrosome amplification. Dot color denotes the mean expression level, and dot size denotes the percentage of expressing cells for each population. (G,H) GSEA analysis between *RACGAP1*$^+$ and *RACGAP1*$^-$ malignant epithelial cells. Avg.Exp, average expression; CIN, chromosomal instability; CNV, copy number variation; GO, Gene Ontology; GSEA, gene set enrichment analysis; NES, normalized enrichment score; Pct.Exp, percent expression; RACGAP1, Rac GTPase-activating protein 1; scRNA-seq, single-cell RNA sequencing; t-SNE, t-distributed stochastic neighbor embedding.

molecular engine indispensable for the orchestration of cytokinesis (25). Based on this, we hypothesized that its overexpression in LUAD drives malignancy via a dual mechanism: driving hyper-proliferation and concurrently inducing chromosomal instability (CIN). Consistent with this hypothesis, differential gene expression analysis showed that *RACGAP1*$^+$ malignant cells markedly upregulate genes controlling cell cycle, cytokinesis, and spindle assembly (*Figure 4D-4F*).

We validated this association in bulk transcriptomes and found a strong positive correlation between *RACGAP1* and established markers of proliferation and CIN (Rs >0.7; Figure S5). Furthermore, GSEA demonstrated that the *RACGAP1*$^+$ signature was associated with hyperactivation of proliferation pathways (E2F targets, G2M checkpoint) (*Figure 4G*). It also revealed a robust DNA damage response

(DDR) signature, a proxy for ongoing genomic stress (*Figure 4G*,*4H*).

Together, these analyses demonstrated that *RACGAP1* orchestrates a malignant cell state defined by a potent combination of hyper-proliferation and CIN.

RACGAP1 orchestrates an apoptosis-resistant proliferative niche in the tumor microenvironment

To resolve the spatial context of *RACGAP1* in LUAD, we generated spatially resolved transcriptomic profiles of the patient-derived tissue. Initial deconvolution of this map using RCTD identified four principal cell lineages (epithelial, NK, T, and B cells) (*Figure 5A*). This analysis revealed that malignant epithelial cells (*EPCAM*$^+$/*KRT8*$^+$) were spatially restricted to dense foci identifiable by histology (*Figure 5B*,*5C*). These foci exhibited high expression of the proliferation marker *CDC20*, establishing them as the primary sites of tumor expansion (*Figure 5C*).

To define the tissue architecture, we applied an unsupervised community detection algorithm. This partitioned the tissue architecture into nine distinct spatial domains. Notably, one community spatially overlapped with the histologically defined malignant region (*Figure 5B-5E*). We designated this unique microenvironment the malignant proliferative niche (MPN) (*Figure 5D*,*5E*). GSEA revealed that MPN upregulates the MYC Target v1 pathway while suppressing p53 signaling and apoptosis (*Figure 5F*). These findings align with the functional characterization of *RACGAP1* from our single-cell transcriptomic analyses.

Functional validation establishes RACGAP1 as a multifunctional driver of proliferation and cell survival

Our multi-omics analyses implicated RACGAP1 as a driver of malignant epithelial states. To formally establish causality and dissect its cellular functions, we engineered A549 LUAD cells for RACGAP1 overexpression (RACGAP1$^+$) and knockdown (shRACGAP1). We confirmed model fidelity at both transcriptomic and proteomic levels (*Figure 6A*,*6B*). Remarkably, RACGAP1 overexpression induced a pro-tumorigenic molecular signature extending beyond cell division control. RT-qPCR and western blot analysis revealed coordinated upregulation of cell cycle regulators (cyclin D1, CDK1) and the DNA replication factor PCNA (*Figure 6C*,*6D*). Concurrently, we observed a fundamental shift in apoptotic balance, characterized by increased anti-apoptotic BCL2 and decreased pro-apoptotic BAX expression (*Figure 6C*,*6D*). Conversely, RACGAP1 depletion produced an inverse molecular profile, confirming the specificity of these oncogenic effects (*Figure 6C*,*6D*). Additionally, compared with their *RACGAP1*-negative counterparts, *RACGAP1*-positive epithelial cells exhibited both a significantly higher mean expression of proliferation-associated markers and a greater percentage of cells expressing these markers (*Figure 6E*).

The molecular reprogramming induced by RACGAP1 translated into profound alterations in cellular behavior. Flow cytometric analysis unveiled the function of RACGAP1 in promoting the G1/S transition. Overexpression significantly reduced G1-phase populations while expanding S-phase populations (*Figure 6F*; Figure S6A,S6B). Conversely, RACGAP1 knockdown induced G1-phase arrest, demonstrating its essential role in cell cycle progression (*Figure 6F*; Figure S6C). These enhanced cell cycle dynamics directly increased proliferative capacity across multiple independent assays. EdU incorporation studies demonstrated accelerated *de novo* DNA synthesis (*Figure 6G*). Similarly, colony formation and CCK-8 assays revealed superior clonogenic potential and enhanced growth rates, respectively (*Figure 6H*,*6I*). Furthermore, Annexin V/PI analysis established a previously unrecognized anti-apoptotic function of RACGAP1. Its overexpression conferred significant resistance to apoptosis, while depletion enhanced susceptibility (*Figure 6J*; Figure S7).

Collectively, these findings establish RACGAP1 as a multifunctional oncogenic driver in LUAD. It promotes malignant progression by simultaneously accelerating cell cycle and suppressing cell death.

Mechanistic dissection reveals that RACGAP1 drives oncogenesis via PI3K/MEK activation and MDM2-linked p53 suppression

To delineate the molecular landscape governed by *RACGAP1*, we analyzed the TCGA-LUAD cohort using GSVA. Consistent with its canonical function in cytokinesis, samples with high *RACGAP1* expression were significantly enriched for proliferation-centric hallmarks, including E2F targets, G2M checkpoint, and mitotic spindle (*Figure 7A*). Beyond this established role, our analysis implicated *RACGAP1* in broader oncogenic networks. Specifically, *RACGAP1* levels correlated positively with PI3K-AKT-mTOR signaling signatures while displaying a robust inverse relationship with p53 pathway activity (*Figure 7A*,*7B*). Notably, *RACGAP1* expression was

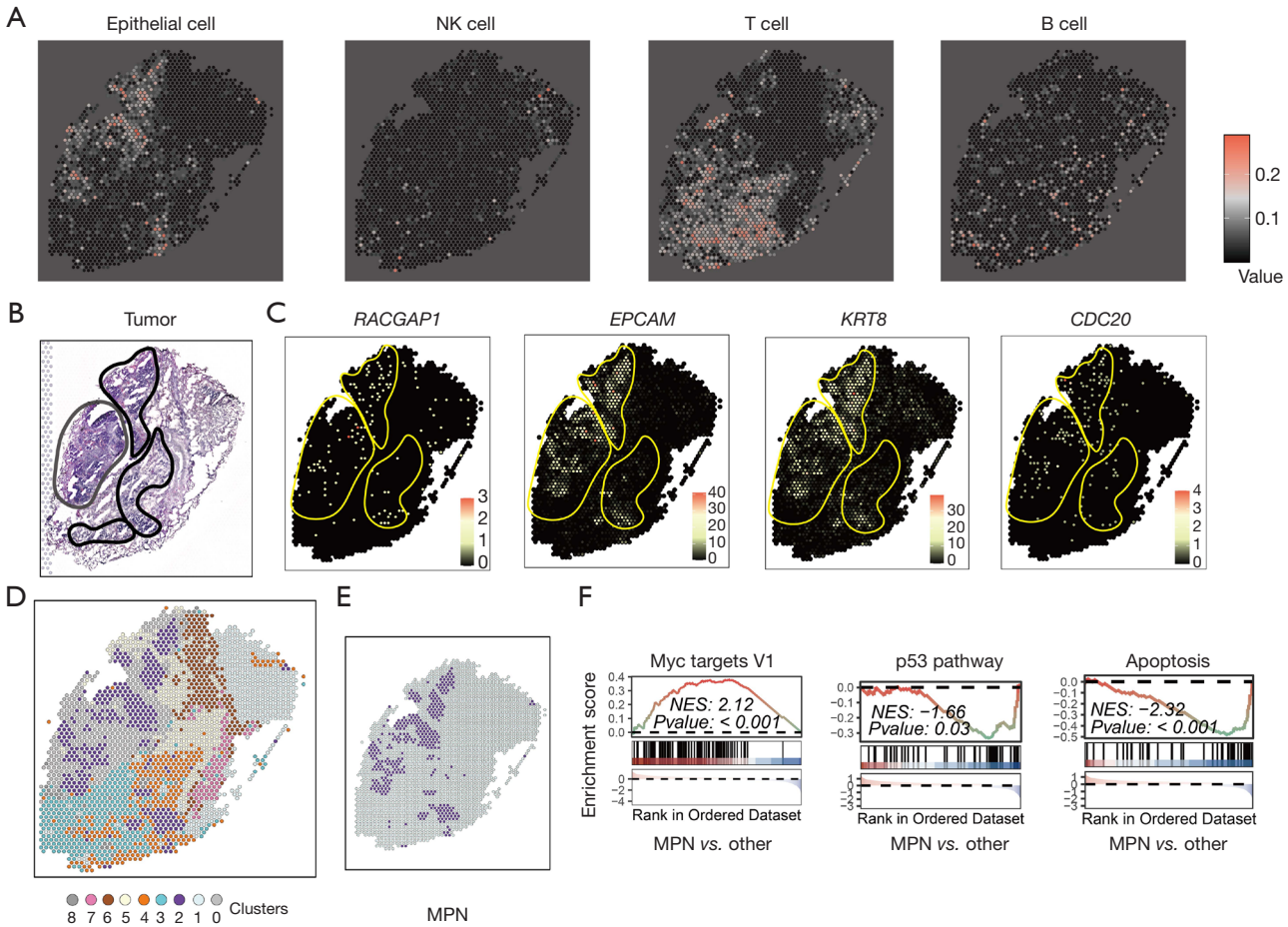

Figure 5 Spatial transcriptomics defines a *RACGAP1*-driven MPN in LUAD. (A) Spatial transcriptomics analysis of a representative LUAD patient. The spatial feature plot illustrates the predicted abundance of cells across the tissue section. Each spot represents a unique spatial location. The color intensity, ranging from grey (low abundance) to red (high abundance), corresponds to the estimated proportion or score of the indicated cell types at that location. (B) H&E staining of the tissue biopsy used for spatial transcriptomics analysis. (C) The spatial distribution of gene expression is visualized across the tissue. Color intensity corresponds to the level of gene expression, as indicated by the scale bar. The yellow outlines highlight specific regions. (D,E) Unsupervised clustering of the spatial transcriptomics partitioned the tissue into nine molecularly distinct clusters. (F) GSEA analysis between MPN and other niches. H&E, hematoxylin and eosin; LUAD, lung adenocarcinoma; MPN, malignant proliferative niche; NES, normalized enrichment score; NK, natural killer; RACGAP1, Rac GTPase-activating protein 1.

negatively correlated with the 'KRAS signaling downregulated' gene set; this depletion serves as a proxy for RAS pathway hyperactivation (*Figure* 7*A*,7*B*). These associations were corroborated by GSEA (*Figure* 7*C*) and further validated by single-cell analysis, where *RACGAP1*$^{+}$ epithelial subclusters recapitulated the pathway alterations observed in bulk transcriptomics (*Figure* 7*D*).

To establish causality, we examined RACGAP1-regulated signaling in LUAD cellular models. Ectopic expression of RACGAP1 triggered the concomitant activation of two principal pro-tumorigenic cascades: the RAF-MEK-ERK (*Figure* 7*E*) and the PI3K-AKT-mTOR pathways (*Figure* 7*F*), as evidenced by increased phosphorylation of their key downstream effectors. Concurrently, RACGAP1 overexpression inactivated the p53 tumor suppressor axis via the upregulation of the E3 ubiquitin ligase MDM2, which promoted the degradation of both total and phosphorylated p53 (*Figure* 7*G*). Conversely, RNAi-mediated depletion of RACGAP1 reversed these signaling alterations, restoring the basal activity of growth pathways and rescuing p53

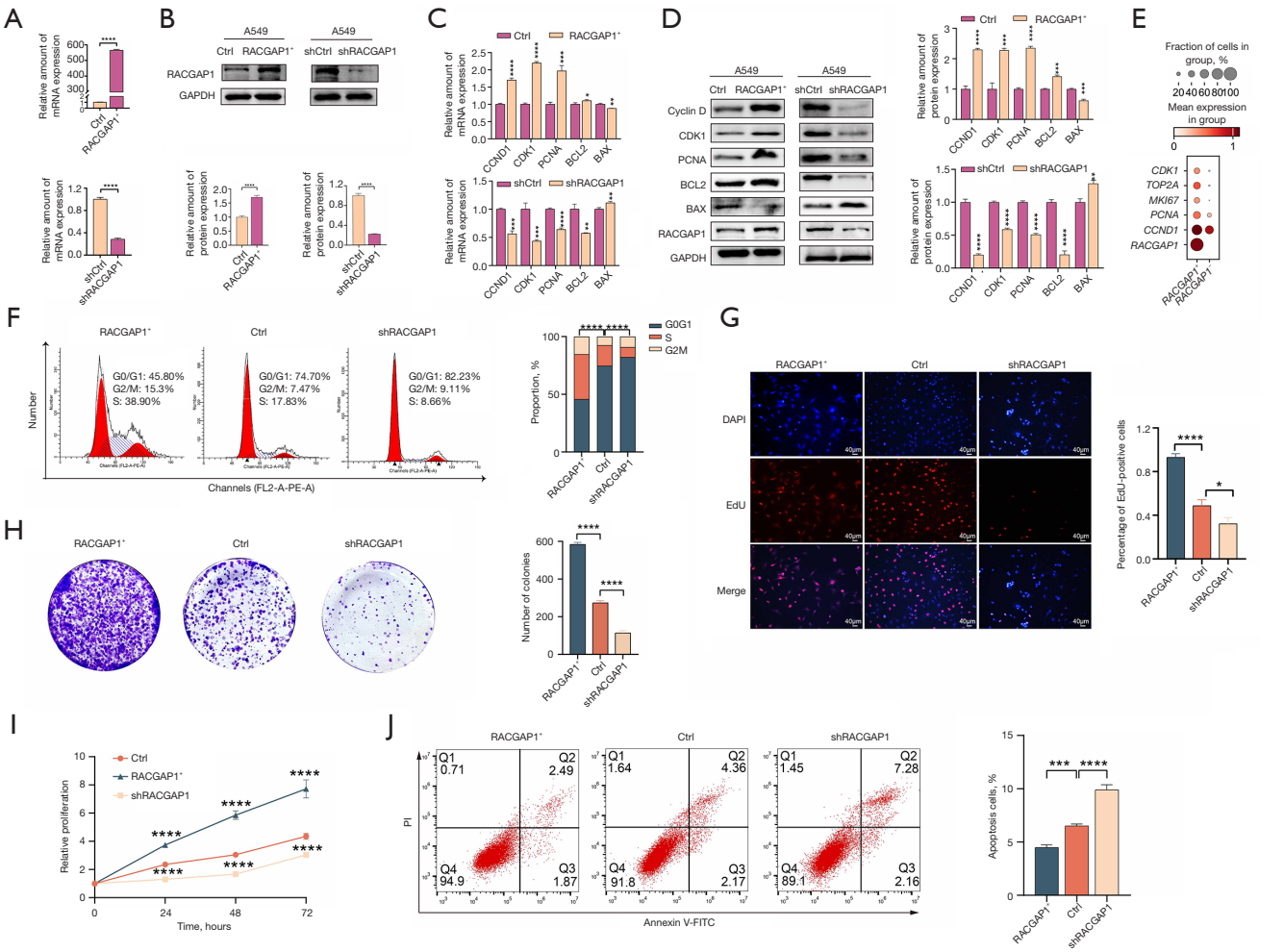

Figure 6 RACGAP1 drives malignant progression in LUAD by promoting cell proliferation and inhibiting apoptosis. (A,B) Established RACGAP1 gain- and loss-of-function models. (C,D) mRNA and protein levels of proliferation and apoptosis-related markers between RACGAP1 gain- and loss-of-function A549. (E) Dot plot showing proliferation markers between *RACGAP1*$^{+}$ and *RACGAP1*$^{-}$ epithelial cells. (F) Flow cytometric analysis showing the cell population in different cell phases. (G) Both knockdown and overexpression of RACGAP1 modulate cell proliferation as revealed by EdU incorporation assay, the proliferating cells were labeled with EdU (red), and the nuclei were counterstained with DAPI (blue). (H) Colony formation assays assess clonogenic potential in A549. Colonies were stained with 0.1% crystal violet. (I) CCK-8 assay shows the viability of control, RACGAP1-knockdown, and RACGAP1-overexpression cells measured at 0, 24, 48, and 72 hours. (J) Effects of RACGAP1 knockdown and overexpression on apoptosis in A549, measured by Annexin V-FITC/PI staining. Data are presented as mean ± SD from at least three independent experiments. Representative images are shown. Statistical significance was determined by a two-tailed Student's *t*-test. *, P<0.05; **, P<0.01; ***, P<0.001; ****, P<0.0001. CCK-8, Cell Counting Kit-8; Ctrl, control; DAPI, 4',6-diamidino-2-phenylindole; EdU, 5-ethynyl-2'-deoxyuridine; FITC, fluorescein isothiocyanate; LUAD, lung adenocarcinoma; mRNA, messenger RNA; PI, propidium iodide; RACGAP1, Rac GTPase-activating protein 1; SD, standard deviation.

expression (*Figure 7H-7J*). Collectively, these results mechanistically establish RACGAP1 as a pivotal oncogenic hub that drives malignant progression by activating PI3K/AKT and MEK/ERK signaling while dismantling the p53 tumor suppressor barrier.

Pharmacological inhibition confirms RACGAP1's dependence on PI3K-AKT-mTOR and MEK/ERK cascades

To validate that these signaling pathways are functionally essential for RACGAP1-mediated oncogenesis, we

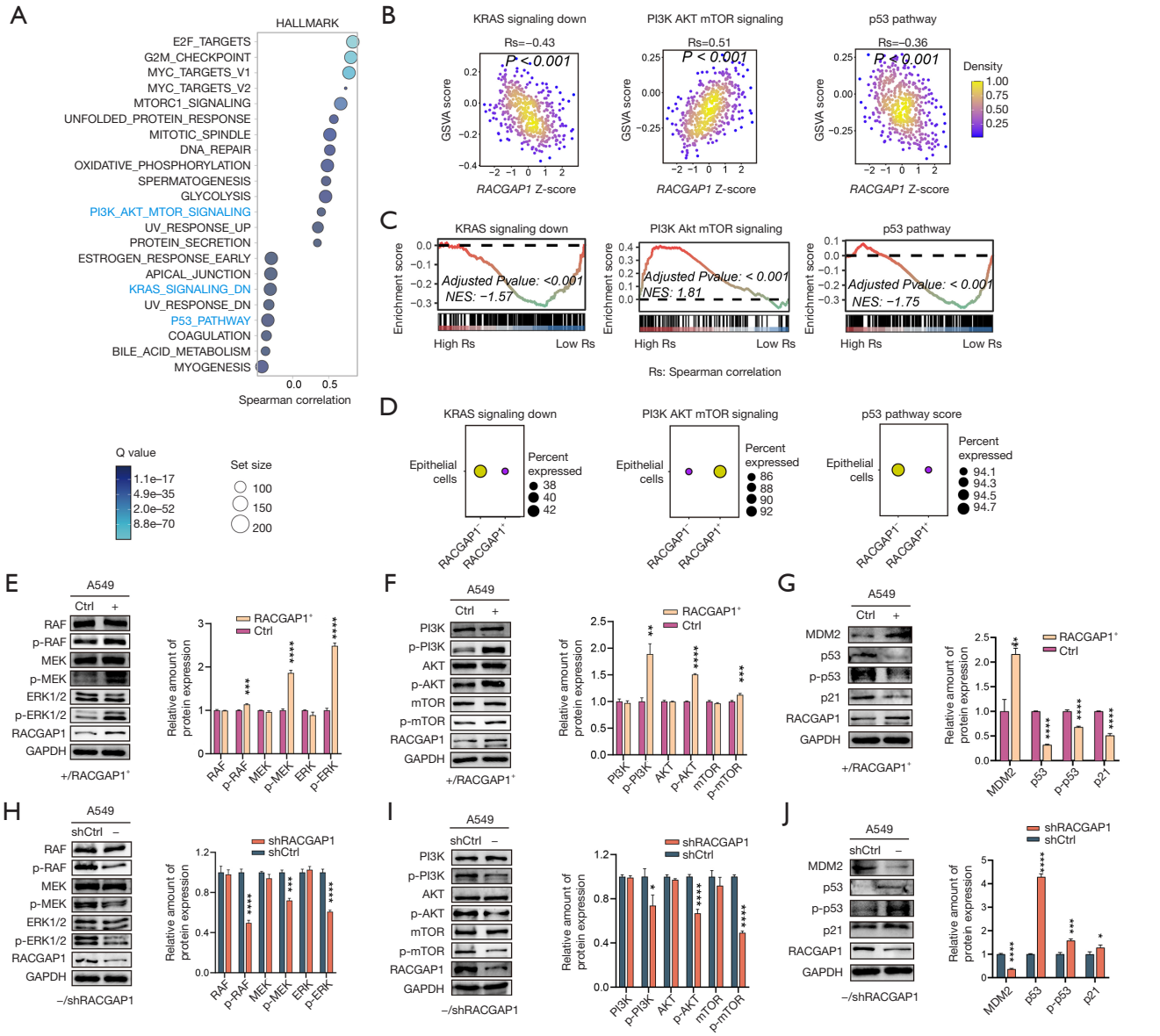

Figure 7 RACGAP1 orchestrates oncogenesis through convergent activation of PI3K-AKT, RAF/MEK/ERK, and suppression of p53 pathways. (A) GSVA showing the enrichment of proliferation-related and oncogenic signaling pathways in TCGA-LUAD samples stratified by *RACGAP1* expression levels. (B) Scatter plot showing the Spearman correlations between *RACGAP1* mRNA gene expression (z score) and GSVA scores for the PI3K-AKT-mTOR, p53, and KRAS signaling pathways in the TCGA-LUAD cohort. (C) GSEA plots validating the significant enrichment of the indicated gene signatures in *RACGAP1*-high tumors. (D) Comparison of pathway activity scores between *RACGAP1*$^{+}$ and *RACGAP1*$^{-}$ epithelial subclusters derived from scRNA-seq analysis. (E-J) Western blot analysis and densitometric quantification of RAF/MEK/ERK (E), PI3K/AKT/mTOR (F), and p53 (G) pathway markers in A549 cells following overexpression of RACGAP1. GAPDH served as the loading control. (H-J) Western blot analysis and densitometric quantification of RAF/MEK/ERK (H), PI3K/AKT/mTOR (I), and p53 (J) pathway markers in A549 cells following knockdown of RACGAP1. GAPDH served as the loading control. Data are presented as mean ± SD from three independent experiments. Statistical significance was determined by a two-tailed Student's *t*-test. *, P<0.05; **, P<0.01; ***, P<0.001; ****, P<0.0001. Ctrl, control; GSEA, gene set enrichment analysis; GSVA, gene set variation analysis; LUAD, lung adenocarcinoma; mRNA, messenger RNA; NES, normalized enrichment score; RACGAP1, Rac GTPase-activating protein 1; scRNA-seq, single-cell RNA sequencing; SD, standard deviation; TCGA, The Cancer Genome Atlas.

employed targeted pharmacological intervention. We treated RACGAP1$^+$ cells with inhibitors of the PI3K-AKT-mTOR pathway (LY294002, MK-2206, rapamycin) and the RAF-MEK-ERK pathway (trametinib). At the molecular level, inhibitor treatment effectively reversed the RACGAP1-induced pro-tumorigenic signature, normalizing the expression of key proliferation markers and restoring the balance of apoptotic regulators (*Figure 8A-8D*; Figure S8). This molecular rescue translated directly into functional outcomes: pathway blockade significantly blunted RACGAP1-driven hyperproliferation (*Figure 8E-8G*) and re-sensitized cells to apoptosis (*Figure 8H,8I*).

These pharmacological rescue experiments provide conclusive evidence that the RACGAP1-driven oncogenic program relies critically on the sustained activity of both the PI3K-AKT-mTOR and RAF-MEK-ERK signaling networks. In summary, our study unveils RACGAP1 as a multifunctional oncogene that transcends its canonical cytokinetic role, orchestrating LUAD progression through convergent pathway activation and offering a rationale for targeted therapeutic strategies.

Discussion

A central challenge in oncology is differentiating the causal drivers of pathogenesis from molecules that are merely disease-associated. To address this, we employed a multi-stage genetic framework that incorporated both colocalization and 2SMR. This integrated analysis provided supportive genetic evidence for the putative causal role of 18 plasma proteins in LUAD risk. Subsequent pathway enrichment analysis revealed that these genetically prioritized proteins were enriched in pathways integral to LUAD pathogenesis.

Following this causal inference, we evaluated the prognostic significance of these 18 proteins. Univariable Cox proportional hazards regression showed that high expression of *RACGAP1*, *GOLM1*, and *CDH17*, and low expression of *CTSH*, were associated with poor overall survival. A subsequent multivariable model refined this, identifying *RACGAP1*, *CTSH*, and *CDH17* as independent prognostic indicators. To ground these findings in tissue-level biology, we then compared transcript and protein levels between tumor and adjacent non-cancerous tissues. This revealed concordant upregulation of RACGAP1 and GOLM1 and downregulation of CTSH at both messenger RNA (mRNA) and protein levels. Notably, the prognostic value of CDH17 was restricted to the transcript level, as its protein abundance was unchanged. Finally, to assess the robustness and generalizability of these findings, we performed multi-cohort validation. We calculated the incremental prognostic value using Harrell's C-index. The addition of *RACGAP1* to a baseline clinical model significantly improved predictive accuracy across multiple LUAD cohorts. These results confirmed RACGAP1 as a consistent and independent predictor of poor outcomes with LUAD, corroborating previous studies (26-29).

Although our bulk-omics studies have implicated *RACGAP1* as an oncogene in LUAD, its specific cellular context and function within the human tumor microenvironment remain unresolved. To address this, we integrated single-cell and spatial transcriptomics to deconstruct their role at a micro-level resolution. By analyzing a high-resolution cellular atlas constructed from 95 clinical samples, we identified a distinct *RACGAP1*$^+$ epithelial cell population that was strongly associated with LUAD progression. These cells exhibited features of CIN, including significant chromosomal aberrations inferred from copy number variations and dysregulation of established biomarkers of CIN (30).

To validate these findings *in situ*, we analyzed the spatial transcriptomics data from patients with LUAD. This analysis revealed a striking spatial colocalization of *RACGAP1*$^+$ cells with pathologist-annotated malignant tumor regions. Furthermore, unsupervised clustering identified a spatial community whose transcriptomic signature—characterized by pro-proliferative and anti-apoptotic features—precisely overlapped with these malignant areas.

Building on this *in situ* identification of *RACGAP1*$^+$ epithelial cells as a key oncogenic niche, we conducted functional experiments to elucidate the underlying molecular mechanisms. Our study uncovered a dual oncogenic program orchestrated by RACGAP1 that extends beyond its canonical role in cytokinesis. We demonstrated that RACGAP1 not only drives cell cycle dysregulation but also confers a potent anti-apoptotic advantage via BCL2/BAX regulation. Mechanistically, we established that RACGAP1 functions as a pivotal signaling hub, concurrently activating the MEK/ERK and PI3K/AKT pathways while dismantling the p53 tumor suppressor axis through MDM2 upregulation. Pharmacological rescue experiments confirmed the critical dependency of RACGAP1's oncogenic functions on these pathways. This dual mechanism suggests that targeting RACGAP1 or its downstream effectors could simultaneously neutralize the two core pillars of cancer—uncontrolled proliferation

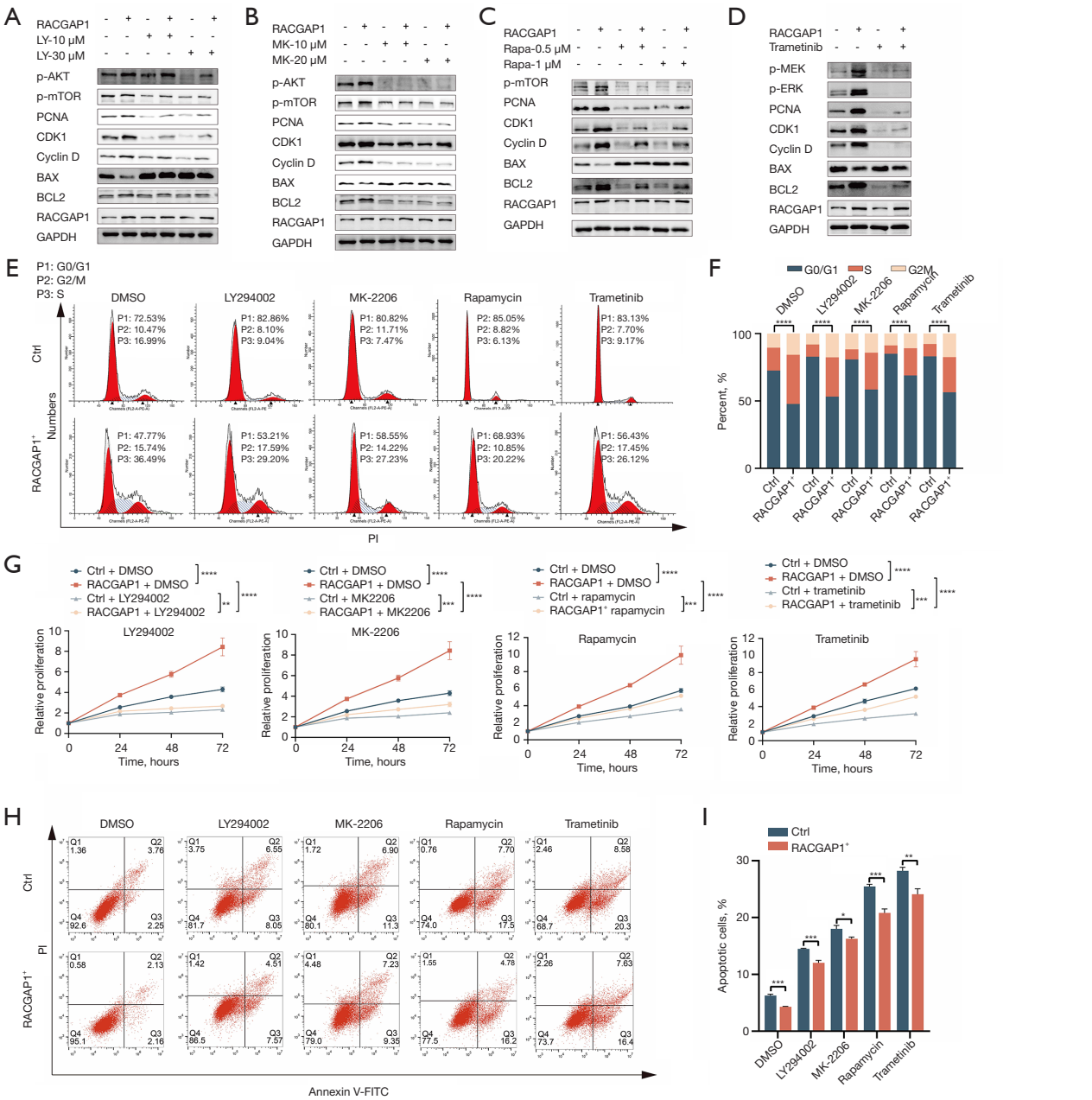

Figure 8 Pharmacological validation confirms RACGAP1's dependence on PI3K-AKT-mTOR and MEK/ERK cascades. (A-D) Western blot analysis in RACGAP1-overexpressing (RACGAP1$^+$) A549 cells treated with inhibitors for the PI3K/AKT/mTOR and MEK/ERK pathways. Cells were exposed to LY294002 (PI3K inhibitor), MK-2206 (AKT inhibitor), rapamycin (mTOR inhibitor), or trametinib (MEK inhibitor). (E) Cell cycle analysis of RACGAP1$^+$ A549 cells treated with the indicated inhibitors. Representative flow cytometry histograms of cell cycle distribution. (F) Quantification of the percentage of cells in the G0/G1, S, and G2/M phases. (G) Cell proliferation of inhibitor-treated RACGAP1$^+$ A549 cells was assessed using a CCK-8 assay. (H) Apoptosis analysis of RACGAP1$^+$ A549 cells post-treatment. Representative flow cytometry plots of cells stained with Annexin V-FITC and PI. (I) Quantification of the total apoptotic rate (early and late apoptotic cells). Data are presented as mean ± SD from three independent experiments. Statistical significance was determined by a two-tailed Student's *t*-test. *, P<0.05; **, P<0.01; ***, P<0.001; ****, P<0.0001. CCK-8, Cell Counting Kit-8; Ctrl, control; DMSO, dimethyl sulfoxide; FITC, fluorescein isothiocyanate; PI, propidium iodide; RACGAP1, Rac GTPase-activating protein 1; SD, standard deviation.

and evasion of apoptosis—offering a powerful therapeutic strategy for LUAD.

While our findings are robust and provide a multi-dimensional characterization of RACGAP1 in LUAD, we acknowledge several limitations that warrant consideration. First, our genetic and MR analyses were primarily based on data from European populations, which may limit the generalizability of our findings to other ethnic groups; validation in diverse cohorts is required to confirm the universality of these associations. Second, regarding experimental validation, our mechanistic conclusions rely on *in vitro* assays using a single cell line. While this provided a controlled system to dissect signaling pathways, it may not fully capture the heterogeneity of LUAD. The lack of *in vivo* validation in animal models is a limitation of the current study, and future work utilizing patient-derived organoids or xenograft models is necessary to confirm these findings in a physiological context. Third, while we elucidated the MDM2-mediated p53 degradation, the precise upstream molecular events through which RACGAP1 modulates the PI3K/AKT and MEK pathways remain to be fully elucidated. Finally, the druggability of RACGAP1 remains to be fully elucidated due to the current lack of specific tool compounds, warranting further investigation to develop selective inhibitors and validate its therapeutic potential.

Conclusions

This study presents genetic evidence supportive of a causal contribution of RACGAP1 to LUAD, highlighting it as a promising prognostic biomarker and candidate therapeutic target. RACGAP1-mediated oncogenic signaling creates a therapeutically exploitable dependency within the MPN identified by spatial transcriptomics. The dual oncogenic mechanism—p53 pathway disruption coupled with pro-survival signaling activation—represents a convergent vulnerability amenable to targeted intervention. These findings provide a foundation for RACGAP1-directed therapies and demonstrate that spatial transcriptomic profiling can guide precision oncology in LUAD management.

Acknowledgments

We would like to express our gratitude to the researchers who generously contributed their original GWASs, single-cell and bulk RNA sequencing datasets to public repositories, thereby enabling our investigations. Additionally, we acknowledge with deep appreciation the developers of open-source R and Python packages, whose sophisticated computational tools proved indispensable to our analytical methodology.

Footnote

Reporting Checklist: The authors have completed the MDAR and STROBE-MR reporting checklists. Available at https://tlcr.amegroups.com/article/view/10.21037/tlcr-2025-aw-1158/rc

Peer Review File: Available at https://tlcr.amegroups.com/article/view/10.21037/tlcr-2025-aw-1158/prf

Funding: This work was supported by a grant from the Sichuan Science and Technology Program (No. 2025ZNSFSC0564).

Conflicts of Interest: All authors have completed the ICMJE uniform disclosure form (available at https://tlcr.amegroups.com/article/view/10.21037/tlcr-2025-aw-1158/coif). All authors report that this work was supported by a grant from the Sichuan Science and Technology Program (No. 2025ZNSFSC0564). The authors have no other conflicts of interest to declare.

Ethical Statement: The authors are accountable for all aspects of the work in ensuring that questions related to the accuracy or integrity of any part of the work are appropriately investigated and resolved. This study was conducted in accordance with the Declaration of Helsinki and its subsequent amendments.

References

1. Han M, Wan F, Xiao B, et al. Cell components of tumor

microenvironment in lung adenocarcinoma: Promising targets for small-molecule compounds. Chin Med J (Engl) 2025;138:905-15.
2. Zhang L, Cui Y, Mei J, et al. Exploring cellular diversity in lung adenocarcinoma epithelium: Advancing prognostic methods and immunotherapeutic strategies. Cell Prolif 2024;57:e13703.
3. Xu J, Tian L, Qi W, et al. Advancements in NSCLC: From Pathophysiological Insights to Targeted Treatments. Am J Clin Oncol 2024;47:291-303.
4. Dong S, Li X, Huang Q, et al. Resistance to immunotherapy in non-small cell lung cancer: Unraveling causes, developing effective strategies, and exploring potential breakthroughs. Drug Resist Updat 2025;81:101215.
5. Huang Q, Li Y, Huang Y, et al. Advances in molecular pathology and therapy of non-small cell lung cancer. Signal Transduct Target Ther 2025;10:186.
6. Banerjee A, Vathiotis I, Halder D, et al. Molecular Landscape and Therapeutic Strategies of Lung Cancer Lineage Plasticity. J Thorac Oncol 2025;20:1582-93.
7. Sun BB, Suhre K, Gibson BW. Promises and Challenges of populational Proteomics in Health and Disease. Mol Cell Proteomics 2024;23:100786.
8. Suhre K, Chen Q, Halama A, et al. A genome-wide association study of mass spectrometry proteomics using a nanoparticle enrichment platform. Nat Genet 2025;57:2987-96.
9. Gupta G, Ali H, Singh SK, et al. Exploring the causal relationship between telomere regulation, aging and neurological disorders. Ageing Res Rev 2026;113:102930.
10. Suhre K. Genetic associations with ratios between protein levels detect new pQTLs and reveal protein-protein interactions. Cell Genom 2024;4:100506.
11. Liu H, Zhu J, Jiang H, et al. Using Mendelian randomization analyses in osteoarthritis: state of art and future perspectives. Ann Med 2025;57:2533428.
12. Salih AM, Salatzki J, Wang Y, et al. Genetic associations of plasma proteomics with dementia subtypes and neuroimaging markers. Alzheimers Dement (Amst) 2025;17:e70202.
13. Chen LG, Tubbs JD, Liu Z, et al. Mendelian randomization: causal inference leveraging genetic data. Psychol Med 2024;54:1461-74.
14. Ferkingstad E, Sulem P, Atlason BA, et al. Large-scale integration of the plasma proteome with genetics and disease. Nat Genet 2021;53:1712-21.
15. Giambartolomei C, Vukcevic D, Schadt EE, et al. Bayesian test for colocalisation between pairs of genetic association studies using summary statistics. PLoS Genet 2014;10:e1004383.
16. Lawlor DA, Harbord RM, Sterne JA, et al. Mendelian randomization: using genes as instruments for making causal inferences in epidemiology. Stat Med 2008;27:1133-63.
17. Burgess S, Thompson SG; . Avoiding bias from weak instruments in Mendelian randomization studies. Int J Epidemiol 2011;40:755-64.
18. Skrivankova VW, Richmond RC, Woolf BAR, et al. Strengthening the Reporting of Observational Studies in Epidemiology Using Mendelian Randomization: The STROBE-MR Statement. JAMA 2021;326:1614-21.
19. Kim N, Kim HK, Lee K, et al. Single-cell RNA sequencing demonstrates the molecular and cellular reprogramming of metastatic lung adenocarcinoma. Nat Commun 2020;11:2285.
20. Wu F, Fan J, He Y, et al. Single-cell profiling of tumor heterogeneity and the microenvironment in advanced non-small cell lung cancer. Nat Commun 2021;12:2540.
21. Sikkema L, Ramírez-Suástegui C, Strobl DC, et al. An integrated cell atlas of the lung in health and disease. Nat Med 2023;29:1563-77.
22. Wu T, Hu E, Xu S, et al. clusterProfiler 4.0: A universal enrichment tool for interpreting omics data. Innovation (Camb) 2021;2:100141.
23. Hänzelmann S, Castelo R, Guinney J. GSVA: gene set variation analysis for microarray and RNA-seq data. BMC Bioinformatics 2013;14:7.
24. Travaglini KJ, Nabhan AN, Penland L, et al. A molecular cell atlas of the human lung from single-cell RNA sequencing. Nature 2020;587:619-25.
25. Simon GC, Schonteich E, Wu CC, et al. Sequential Cyk-4 binding to ECT2 and FIP3 regulates cleavage furrow ingression and abscission during cytokinesis. EMBO J 2008;27:1791-803.
26. Mosca N, Pezzullo M, De Leo I, et al. RacGAP1 Plays an Oncogenic Role in Lung Adenocarcinoma by Regulating the Wnt/β-Catenin Pathway. Cells 2025;14:773.
27. Xu Q, Li J, Zhuo L, et al. RACGAP1 is a pivotal gene in lung adenocarcinoma-associated membranous nephropathy: Based on comprehensive bioinformatics analysis and machine learning. Int Immunopharmacol 2024;139:112783.
28. Lai W, Su Y, Li Y, et al. Elevated RACGAP1 Expression Enhances Malignant Potential in Lung Adenocarcinoma and Serves as a Prognostic Factor. J Cancer

2024;15:4244-58.
29. Liu Y, Han T, Miao R, et al. RACGAP1 promotes the progression and poor prognosis of lung adenocarcinoma through its effects on the cell cycle and tumor stemness. BMC Cancer 2024;24:7.
30. Carter SL, Eklund AC, Kohane IS, et al. A signature of chromosomal instability inferred from gene expression profiles predicts clinical outcome in multiple human cancers. Nat Genet 2006;38:1043-8.

Cite this article as: Yi M, Shi J, Xie S, Tao D, Su Z, Yang Y, Liu Y. RACGAP1 defines a malignant proliferative niche and represents a therapeutic vulnerability in lung adenocarcinoma. Transl Lung Cancer Res 2026;15(1):12. doi: 10.21037/tlcr-2025-aw-1158